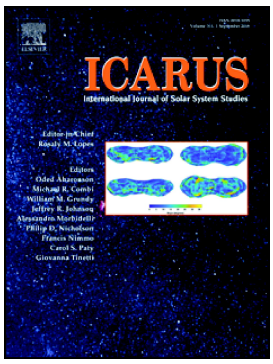

Craters as sand traps: Dynamics, history, and morphology of modern sand transport in an active Martian dune field

K.P. Roback, K.D. Runyon, J.P. Avouac

PII: S0019-1035(19)30627-X

DOI: https://doi.org/10.1016/j.icarus.2020.113642

Reference: YICAR 113642

To appear in: *Icarus*

Received date: 10 September 2019

Revised date: 17 December 2019

Accepted date: 14 January 2020

Please cite this article as: K.P. Roback, K.D. Runyon and J.P. Avouac, Craters as sand traps: Dynamics, history, and morphology of modern sand transport in an active Martian dune field, *Icarus*(2020), https://doi.org/10.1016/j.icarus.2020.113642

Craters as sand traps: Dynamics, history, and morphology of modern sand transport in an active Martian dune field

Roback, K. P.[1], Runyon, K. D.[2], and Avouac, J. P.[1]

[1] – California Institute of Technology, Division of Geological and Planetary Sciences

[2] – Johns Hopkins University Applied Physics Laboratory

Abstract

Aeolian transport of sand is abundant on modern-day Mars, as revealed by remote sensing measurements of the motion of dunes, and of the meter-scale ripples that mantle them. We study a large-scale natural sand trap within the Meroe Patera dune field: a 1.8-km diameter crater which features a dune-free "shadow" in its lee. We compare the volume of sand trapped within this crater to the sand volume that would be expected to cover the area of the crater and its dune-free shadow behind it if the crater were not present. We find that the crater holds less sand than this "missing" volume would predict, implying that sand escapes from the crater over time. Modern day imagery shows an apparent lack of sand escaping from the Meroe crater, however, suggesting that changes in the wind regime at the site may have allowed sand to escape in the past. The persistence of an altered dune morphology all the way to the far downwind edge of the dune field suggests consistent wind conditions over the time of the crater-dune field interaction.

Introduction

Dune fields are common features on Mars [e.g., *Hayward et al.* 2014], and active sand transport has been observed at many different locations [*Banks et al.* 2018; *Chojnacki et al.* 2019; *Silvestro et al.* 2010, *Bridges et al.* 2012, *Ayoub et al.*

2014, *Runyon et al.* 2017a,b]. Cycles of aeolian erosion and deposition appear to be a dominant mechanism driving landscape evolution on modern-day Mars [e.g., *Runyon et al*., 2017b].

Windblown sand moves in varying modes [e.g., *Anderson*, 1987]; while saltation on Mars is energetic with long hop lengths, other grains move via the slower and less-energetic processes of reptation and creep [*Andreotti,* 2004; *Almeida et al.,* 2008; *Sullivan and Kok*, 2017]. As a result of these varying energy levels, bedforms of different scales express different fluxes of sand grains; an example of this appears in the comparison of sand fluxes measured at ripples to the sand fluxes measured from motion of whole dunes; the much lower ripple fluxes largely represent only the portion of sand grains moving in reptation and creep [*Bridges et al.* 2012, *Ayoub et al.* 2014; *Lapotre et al*., 2018].

Accurate estimates of total sand flux are crucial for understanding the depositional and erosional geologic histories of various parts of the planet, yet no direct flux measurement on Mars using in situ sand traps has ever occurred. For the first time, we use an intra-dune field impact crater as a natural sand trap to further explore the dynamics of sand transport on the Martian surface.

Setting and morphology of the Meroe dune field

We focus on the Meroe Patera dune field, an actively migrating barchan dune field and downwind sand sheet located north of the Martian equator in the Syrtis Major region at 7.16 N, 67.75 E (Fig. 1). The field is located in the midst of a largely flat plain 36 km from the Meroe Patera caldera. The region has been mapped as an

early Hesperian volcanic unit densely crossed by tectonic lobate scarps [*Tanaka et al.,* 2014].

The dune field is dominated morphologically by barchan dunes, and barchanoid ridges formed by merging barchan dunes. The primary slipface orientation is towards the west-southwest. The southerly horns of the barchans are consistently extended relative to the northern horns, suggesting the influence of a secondary wind regime oriented in a more southerly direction than the net sand transport direction indicated by the barchans' overall geometry; the dunes are in the "fingering mode" of *Courrech du Pont et al.* (2014).

Crater-Dune Field Relationship

Within the Meroe Patera dune field, a 1.8 km-diameter, 350 m deep impact crater serves as our natural sand trap (Fig. 2). We have unofficially nicknamed it Nathan's Crater, after our late collaborator Nathan Bridges who inspired much of the present work. A dune-free shadow stretches ~2.6 km downwind of the crater's rim (Fig. 1). HiRISE imagery of the crater itself reveals a large quantity of sand trapped within the crater, with more actively entering over the crater's upwind, eastern rim (Fig. 2). No surficial crater ejecta is observed anywhere around the crater, and on the downwind (western) side of the crater, only exposed bedrock is apparent. No large sand sheets or dunes appear to be exiting from the crater. The crater thus appears to act as a sand trap.

The shape and the length (~2.6 km) of the dune-free shadow could suggest that the crater postdates the dune field. In other words, the impact could have punched into the dune field; in this model the dune-free shadow would open and

lengthen over time as the dunes which survived the impact on its downwind side migrated away from the crater. We do not favor this interpretation, given the apparent absence of a fresh ejecta facies surrounding the crater, the presence of many superimposed meter-scale craters near and within Nathan's Crater (Fig. 4), and the very low likelihood that the dune field would have survived the creation of a ~2-km diameter crater. Some basic crater statistics performed <500 m from the crater rim finds densities of ≥20 m diameter craters on the order of 100/km^2; this supports a surface age, given current Martian isochrons [*Hartmann*, 2017] on the order of 100 Ma or greater (Fig. 5), far too old to postdate the dune field's likely arrival. We therefore conclude that the crater was already present when the leading (downwind) edge of the dune field arrived at its location, assuming the dune field is migrating *en masse* (Fig. 6). The downwind edge of the dune field is ~7 km downwind of Nathan's Crater, but a sand sheet extends beyond the dunes to ~13 km downwind.

We estimate the volume of sand $\mathbf{v_{crater}}$ trapped within this crater, and compare it to the volume $\mathbf{v_{shadow\_min}}$ of sand that we would expect to be present if the crater and its dune-free shadow did not exist (Fig. 6), and were instead covered with dunes of the same spatial density and morphology as those that exist elsewhere in the dune field. Comparing these volumes reveals the crater's effectiveness as a sand trap to integrate past sand fluxes and possibly records the presence of earlier dune fields. If the volume of trapped sand $\mathbf{v_{crater}}$ is significantly greater than the volume of missing sand $\mathbf{v_{shadow\_min}}$, this could imply trapping of a population of sand grains which avoid being trapped in dune slipfaces, but cannot

avoid trapping by Nathan's Crater. These grains would need to move in long hops to avoid trapping in dune slipfaces, and might particularly include any grains traveling in suspension. Alternatively, this could indicate the presence of a "leftover" volume of sand from earlier generations of dune fields which passed by the crater.

If $\mathbf{v_{crater} < v_{shadow\_min}}$, this would imply that the crater has not been a completely effective sand trap over long timescales, and that a significant fraction of the sand that passed the crater escaped downwind or never entered it. The volume of sand in the crater can also be compared to the total volume of sand ($\mathbf{v_{shadow\_max}}$) that should have accumulated from the dunes falling into the crater since the leading edge of the dune field first reached it. This total volume of sand can be estimated by projecting the crater diameter to the far downwind edge of the dune field, and estimating the volume of sand ($\mathbf{v_{shadow\_max}}$) that would be expected to cover this area if its sand supply had not been disrupted by the crater's presence. $\mathbf{v_{shadow\_max}}$ can alternatively be calculated by using modern dune migration rates and morphology to estimate a long-term bulk sand flux into Nathan's Crater; this can be multiplied by the length of time the dune field has been present at the crater assuming steady *en masse* migration of the dune field to derive an estimate of the total input volume $\mathbf{v_{shadow\_max}}$. This input volume neglects the possibility that the dune field's migration rate $\mathbf{c_{field}}$ is different from the migration rate of individual dunes, $\mathbf{c_{dunes}}$.

If $\mathbf{c_{field} < c_{dunes}}$, this would imply that dunes should form at the dune field's upwind edge, and that at the downwind margin of the dune field dunes should decay out of existence as they migrate. In this scenario, the timescale of crater-dune field

interaction could be much longer than assumed, causing the longterm input sand flux to Nathan's Crater to be much higher. Alternatively, if $\mathbf{c_{field} > c_{dunes}}$, we would expect dunes at the upwind margin to be steadily decaying through time, losing sand through barchan horns to be organized into dunes further downwind.

Our current timeseries of HiRISE images at Meroe Patera is insufficient to provide a strong argument in favor of any of these particular dynamical scenarios, although the lack of visible protodunes on the Meroe dunefield's upwind edge does suggest that the $\mathbf{c_{field} < c_{dunes}}$ scenario is unlikely. The smaller, less well developed dunes on the dune field's downwind edge might be interpreted as either decaying dunes or developing protodunes. Longer timeseries of imagery at Meroe would likely reveal upwind dune formation or shrinkage, enabling this distinction to be better resolved in later studies.

Dune Motion Measurement

We measured the migration rate $\mathbf{c_{dunes}}$ of the dunes by tracking the changing positions of dune slipfaces relative to bedrock in timeseries of co-registered and orthorectified high resolution (0.25-0.5 m/pixel) orbital High Resolution Imaging Science Experiment [HiRISE*; McEwen et al*. 2007] images. We processed the images in the ENVI plug-in Co-registration of Optically Sensed Images and Correlation [COSI-Corr; *Leprince et al.* 2007]. We multiplied the migration rate of each individual dune with its average height, equivalent to the moving sand thickness, to estimate sand flux associated with whole-dune migration (Fig. 7). We used a 1-m post-spacing three-dimensional HiRISE digital elevation model (DEM) generated from images ESP_050939_1875 and ESP_051084_1875. Using HiRISE images, we mapped

out sand-covered and sand-free parts of the Meroe Patera dune field, and extracted elevations from the DEM over sand-free areas. We projected the bedrock surface under the dunes to generate an interpolated continuous bedrock surface, which we subtracted from the DEM. This subtraction of bedrock topography from total topography allowed an accurate estimate of dune volume in order to represent it as an equivalent sand thickness everywhere in the dune field (Fig. 7).

Trapped Sand Volume Measurements

To estimate the volume of sand ($\mathbf{v_{crater}}$) trapped within Nathan's Crater, we use the same 1-m resolution HiRISE DEM described previously. We extract radial wall profiles extending outwards in all directions from the center of the crater, covering the sand-covered and sand-limited parts of the crater's walls. We then average wall profiles extracted over sand-covered and sand-free areas to derive an average representative profile for each part of the crater (sand-covered and sand-limited) (Fig. 8). We compare these profiles to derive an estimate of average sand thickness in the sand-covered portion of the crater, assuming an axisymmetric bedrock geometry under the sand.

We estimate the uncertainty on this measurement of sand depth and test our assumption of axisymmetric geometry by repeating this analysis for sand-free craters for which we have HiRISE DEM data available (Table 1). The apparent volume of trapped sand in these craters derived from our method should be zero within the measurement uncertainty. We extract radial wall profiles from these craters, and cut the craters in two halves. We then derive representative wall profiles for these sections and compare them, calculating the standard deviation of

the along-profile elevation differences for each pair of representative profiles. For each crater, we rotate the choice of the two sections, and compare representative profiles for each, to account for possible variability in the profiles depending on which part of the crater is considered. While the sand-free craters we measure are not the same size as Nathan's Crater, their proportions are similar and all were simple craters with diameters on the scale of 1 km (Table 1).

Additionally, the floor of Nathan's crater, a flat area ~440 m in diameter, is covered with sand of an unknown thickness. This thickness is likely to be minimal (<10 m), given the observed shallowing of slopes near the bottom of the crater's mostly sand-free western wall. Nathan's Crater has a depth to diameter (d/D) ratio of 0.19, which is typical for unfilled simple craters (e. g., *Melosh*, 1989) and implies a degree of sand infill that is minimal in comparison to the crater's overall depth. We assume 1 m as a low bound, and 10 m as a high-end bound for the thickness of sand mantling the crater's flat floor.

By subtracting the measured crater topography from the expected bedrock topography, we find that the thickness of sand mantling the crater's walls is 11.2 m. We constrain a 2-sigma (95% confidence) uncertainty on this measurement, from our investigation of wall profiles of sand-free craters, of 6.5 m. The 2-sigma confidence interval is defined as the along-profile-averaged difference in elevation greater than or equal to that observed in 95 percent of tested pairs of halves of sand-free craters. By adding this sand volume to our maximum and minimum estimates of sand volume on the crater floor, we derive a volume of trapped sand ($\mathbf{v_{crater}}$) within Nathan's Crater of 7.52×10^6 – 2.95×10^7 m^3.

Comparison with the 'missing' volume of sand in the crater shadow

Next, we estimate the volume of sand that we'd expect to see covering the area of Nathan's Crater and its dune-free shadow if the crater were not present ($\mathbf{v_{shadow\_min}}$). This volume is a minimum estimate of $\mathbf{v_{shadow\_max}}$, the total volume of sand input to Nathan's Crater, given the likelihood that some sand has spread into the shadow from its sides. To derive this volume, we multiply the area of the crater and its shadow by a representative averaged sand thickness for the Meroe Patera dune field. We calculate this thickness using the previously described method from HiRISE DEM data. To assess possible variability in sand thickness on the kilometer-width scale of the crater and its dune free shadow, we calculated averaged sand thicknesses in test windows of the same size and geometry as the crater and its shadow, placed on either side of the sand shadow.

The corresponding "missing" volume $\mathbf{v_{shadow\_min}}$ from the crater's dune-free shadow is 6.22 – 7.92 x 10^7 m^3. The volume of sand in the crater is about 47-91% lower than the missing volume. This relation implies that the crater is unlikely to be trapping any additional flux of sand that is not being captured by the sand dunes themselves, and thus may not record the passage of previous generations of dune fields. By contrast, a fraction of the sand that was trapped in the crater likely escaped downwind or never entered the crater in the first place due to deflection by the topography of the raised rim.

Long-term Sand Input into Nathan's Crater

Dunes at Meroe Patera migrate an average of 0.5 ± 0.22m (2-sigma) per Earth year, with a range from ~0.1 to 1 m per Earth year. The average whole-dune

sand flux observed at Meroe Patera is ~7 m^3/m/Earth yr, with maximum fluxes (migration rate multiplied by maximum dune height) of 11.5 m^3/m/Earth yr. We can estimate the sand flux these dunes deposit into the crater by multiplying the whole-dune flux by the fraction of the dune field area covered by dunes (0.6), and the diameter of the crater; the bulk sand flux associated with dunes alone is estimated to be 4.2 m^3/m/Earth year, with an associated flux into the crater of 7600 m^3/Earth year. We assume that the inter-dune sand flux is 1/3 of the maximum flux [*Ould Ahmedou et al.* 2007]. This interdune flux is accordingly multiplied by the fraction of the dune field area not covered by dunes (0.4), to derive a total interdune flux of 1.5 m^3/m/Earth year. We add this interdune flux to the whole-dune flux to estimate a bulk flux for the Meroe Patera dune field of 5.7 m^3/m/Earth year. Given the crater's diameter of 1.8 km, we estimate a sand flux into the crater of 10300 m^3/Earth year.

The current migration rates of dunes $\mathbf{c_{dunes}}$ at Meroe Patera can be combined with measurements of the dune field's size to estimate the likely timescale of dune activity at Nathan's Crater, under the assumptions of consistent wind conditions over the timescale of dune activity at Nathan's Crater, and *en masse* migration of the dune field at a rate $\mathbf{c_{field}} = \mathbf{c_{dunes}}$ as the migration rate of individual dunes. The downwind edge of the Meroe Patera dune field is about 7 km downwind of Nathan's Crater, and a sand sheet extends to about 13 km downwind. Given the dunes' observed migration rate of ~0.5 m per Earth year, and these measured distances, the upwind arrival of the dune field would have happened about 14,000-26,000 Earth years ago.

By multiplying the sand flux into the crater by the estimated timescale for dune activity at Nathan's Crater of ~14,000-26,000 Earth years, we can estimate the total sand volume $\mathbf{v_{shadow\_max}}$ that has entered the crater, assuming constant climate over the history of the dune field at this site and that all passing sand has been trapped in the crater. This volume is 1.35 - 2.5 x 10^8 m^3, much larger than our estimate of the volume of sand $\mathbf{v_{crater}}$ trapped within the crater.

Alternatively, we can estimate $\mathbf{v_{shadow\_max}}$ by multiplying our observed averaged sand thicknesses by the entire area of the "shadow" downwind of the crater, indicated schematically by the area between the dashed lines in Fig. 6. This includes those areas which are now covered by dunes due to lateral spreading of sand into the shadow. From this, we estimate a total input volume of sand of 1.06 – 2.5 * 10^8 m^3, similar to our time-based estimate of total input flux into the crater.

Thus, we estimate that the trapped sand volume $\mathbf{v_{crater}}$ in Nathan's Crater is only 15 ± 12% of the likely input volume $\mathbf{v_{shadow\_max}}$. Furthermore, these estimates of total input volume assume *en masse* migration of the whole dune field through time; if the dune field is not migrating in this matter, it could have persisted at Nathan's Crater for a much longer period of time, meaning that the actual long-term input sand volume could be much higher than we estimate.

The paucity of sand trapped within Nathan's Crater, relative to our estimates of the likely input volume it has received through time, could arise from two broad mechanisms. Firstly, it is possible that sand that has entered the crater has has been blown out over time. Alternatively, it is possible that passing sand may never enter the crater. We favor the first explanation over the second, due to a lack of

morphological evidence for deflection of sand around the crater's raised rim. Mapping of dune brink lines around Nathan's Crater shows no evidence of deflection of the motion of oncoming dunes by the crater's rim (Fig. 9), and several dunes are observed to be actively climbing up over and falling into the crater in HiRISE images. This result should not be taken as a surprise, given that the slopes surrounding the exterior of Nathan's Crater's rim are low (~10 degrees), and active climbing dunes are observed on 15-degree slopes in Valles Marineris (*Chojnacki et al.,* 2010). While the deflection of small portions of the input sand volume entering the crater rim near its northern and southern extremities cannot be ruled out, it is highly unlikely that the required majority of the input sand volume has been lost in this way given the modern dune morphologies observed near Nathan's Crater.

We thus believe that Nathan's Crater, despite its appearance as a crater with rapid input and little visible output of sand in HiRISE images, is not an effective trap of sand over long timescales. This discrepancy might imply past change in the wind regime at the crater, or the occurrence of past extreme sand transport events. Alternatively, strong winds impacting the upwind-facing crater wall could rapidly transport sand over and away from the wall, preventing accumulation of sand and bedform formation despite possibly significant fluxes.

Notably, the dunes downwind of the crater, even in the zone where dunes have reappeared, are smaller and more widely spaced than those found in other nearby parts of the dune field (Fig. 1), implying that a more limited sediment supply persists to the downwind edge of the dune field, likely due to sand trapped by the crater. The persistence of this altered morphology implies a consistent direction of

the dominant sand transport since the dune field reached the crater and began depositing sand there. Our observation of effective long-term escape of sand at Nathan's Crater supports past studies of central mounds in much larger craters, such as Gale [e. g., *Kite et al.,* 2013; *Day and Kocurek,* 2016], which have invoked aeolian infill and exhumation as their formation mechanisms. However, the question of how extensive aeolian infilling of craters might occur at all, given the apparent difficulty of maintaining infill at this site, remains unresolved. Our results suggest that sand can be effectively removed from Martian craters over long timescales.

Conclusions

We investigate the effectiveness of sand trapping by an intra-dune field Martian crater by measuring its volume of trapped sand, and compare it to the amount "expected" to be in the crater, based on observed sand thicknesses at the dune field and the size of the crater and a dune-free shadow extending downwind. The morphology of the shadow, the dunes downwind of it, and the dune migration rate, imply a consistent direction of sand transport at Meroe Patera for ~10,000 Earth years or longer. We find that the trapped volume is 85 ± 12% less than the expected volume, suggesting that the crater "leaks" sand downwind and is only partially successful at trapping it. While at first the crater appears to be an effective trap with minimal escape of sand in the present day, this appearance may simply be a result of strong winds leading to a lack of sand accumulation and possible rapid transport on the crater's downwind wall. Thus, the sand in Nathan's Crater sets a lower bound on the volume of passing sand. Our work sets the stage for the use of craters as sand traps elsewhere on Mars, Venus, and Titan in order to better

understand the mechanics and histories of sand transport reflected in planetary aeolian environments.

Acknowledgements

This work was supported by funding from the King Abdulaziz City for Science and Technology, and from NASA Grant NNX16AJ43G/123117. We honor the memory of our prematurely late colleague, Nathan Bridges, who inspired the present work by occasionally mentioning, "there might be something to those crater sand shadows, but I'm not sure what." We also thank Dr. Mackenzie Day and an anonymous reviewer for their helpful reviews and comments.

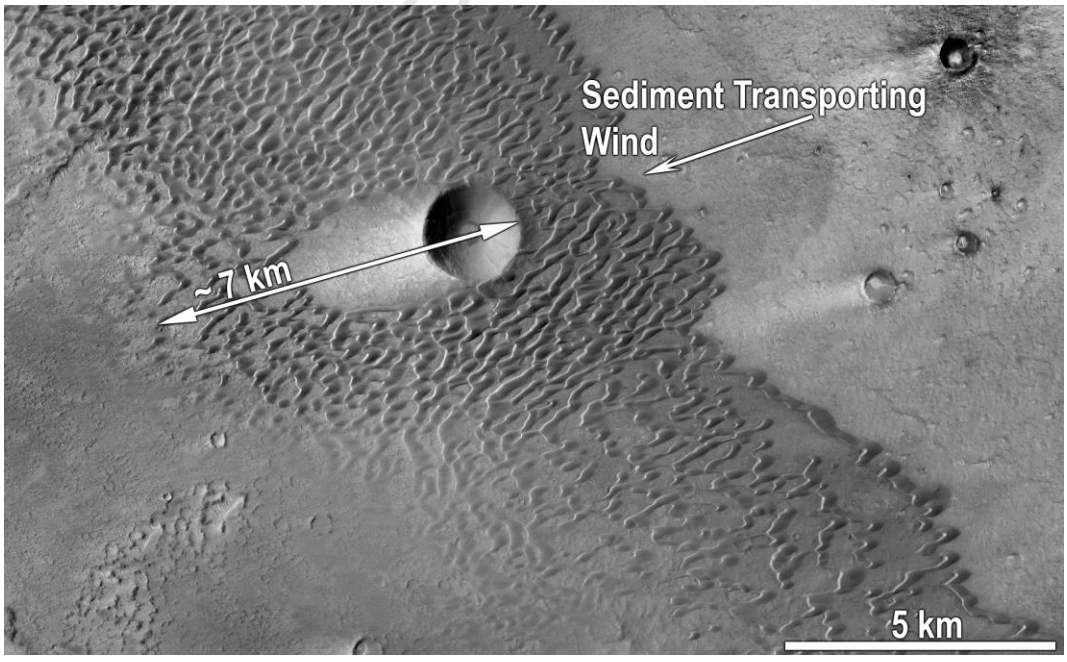

Fig. 1: CTX imagery of the Meroe Patera barchan dune field, annotated to indicate the dominant wind direction implied by the barchans' morphology. Image Credit: NASA/JPL/MSSS.

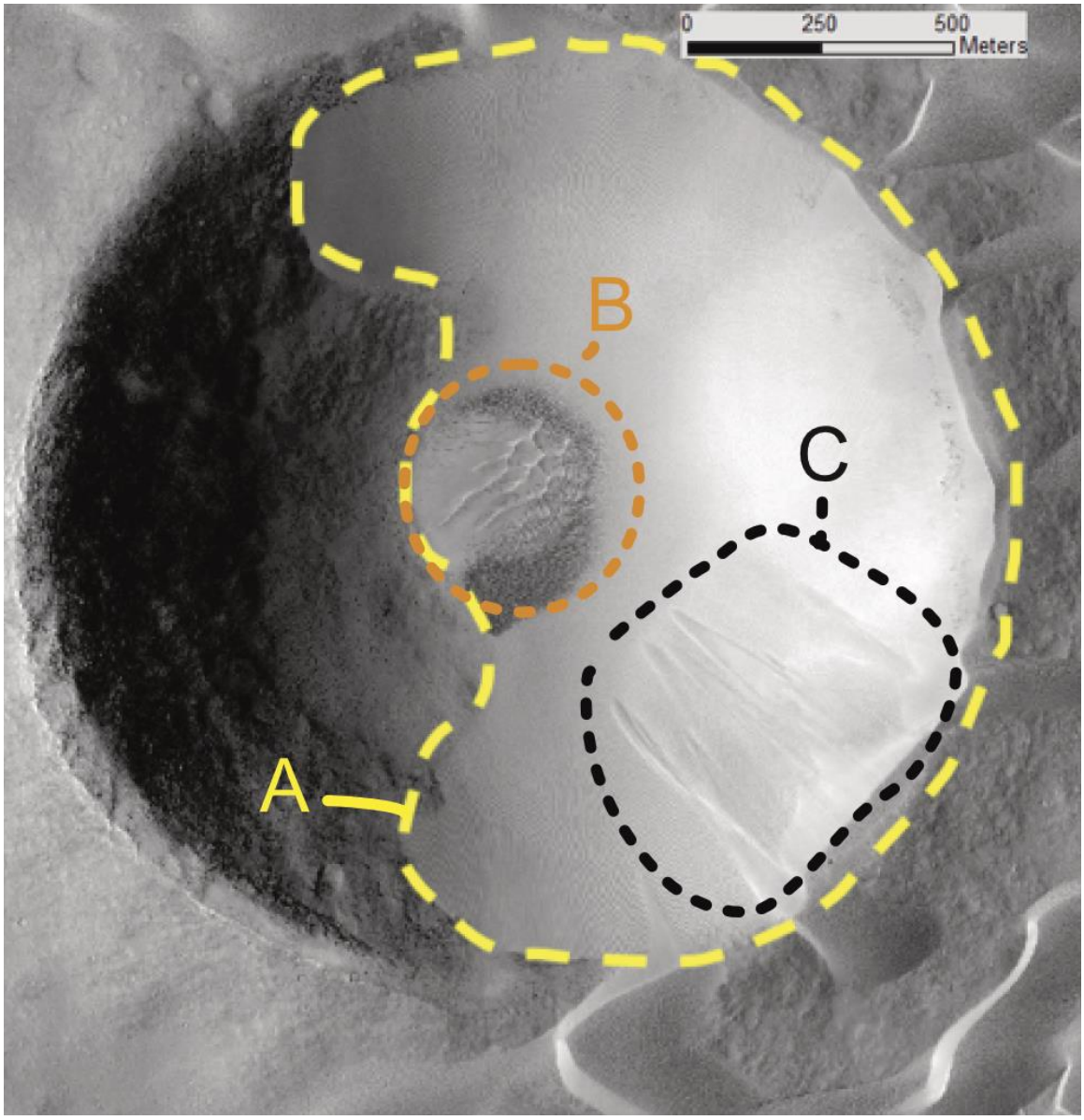

Fig. 2: HiRISE image ESP_050939_1875 of Nathan's Crater, annotated to highlight relevant features. A) Outline of the sand-covered portion of Nathan's Crater. B) Area of transverse aeolian ridges on the sand-covered floor of Nathan's Crater. C) Visible grainfalls illustrating modern infill of aeolian sand to Nathan's Crater. HiRISE image credit: NASA/JPL/University of Arizona.

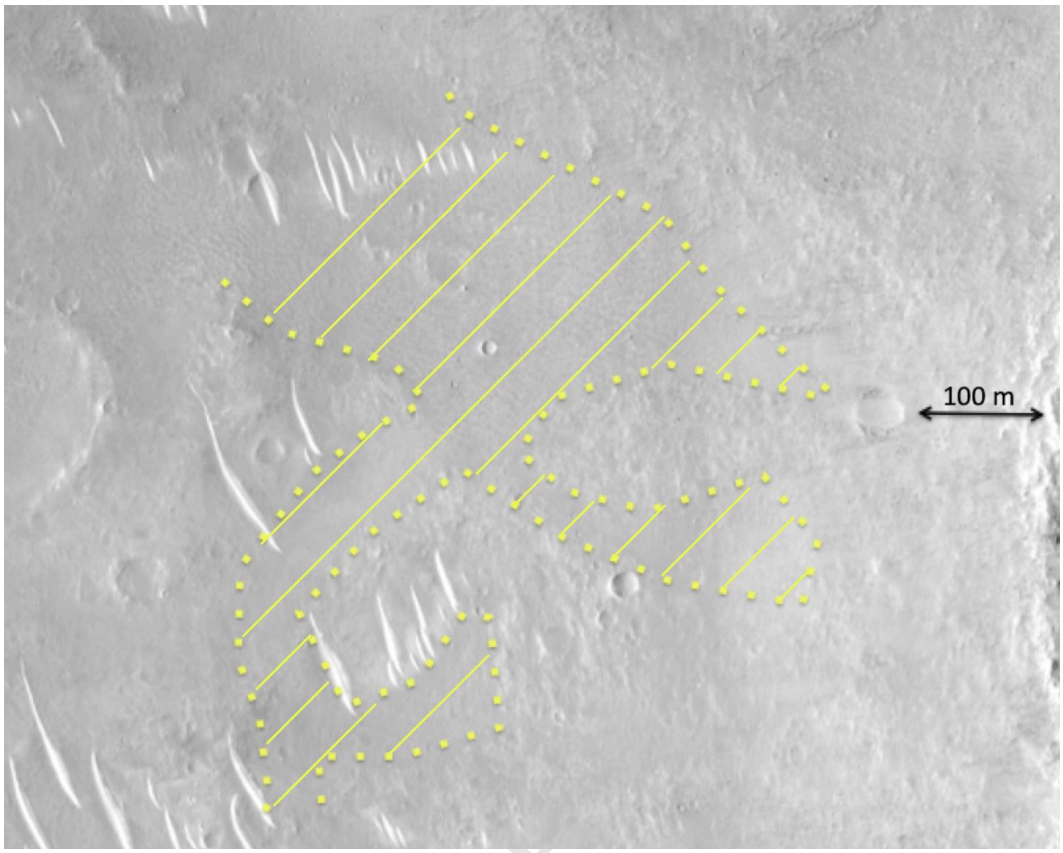

Fig. 3: HiRISE imagery of a portion of the dune-free shadow just downwind of the crater, showing the presence of limited volumes of sand cover (outlined yellow area). The sand shows a faint ripple pattern, but also is the same albedo as the surrounding bedrock, implying that it is dusty and at present immobile.

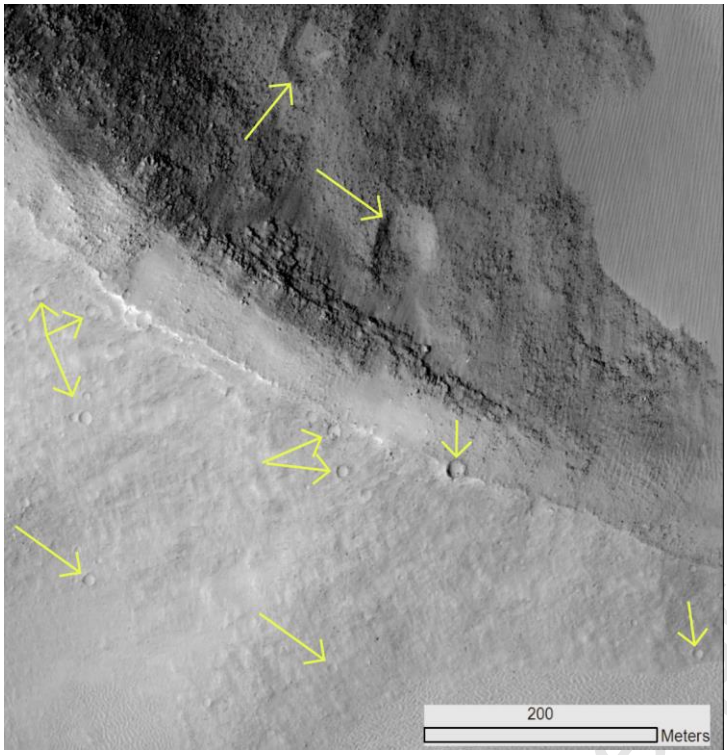

Fig. 4: HiRISE imagery of the southwest part of the crater rim, with some superposed younger craters indicated by arrows. There is also a general lack of ejecta around this crater, indicating its relatively old age. HiRISE image credit: NASA/JPL/University of Arizona.

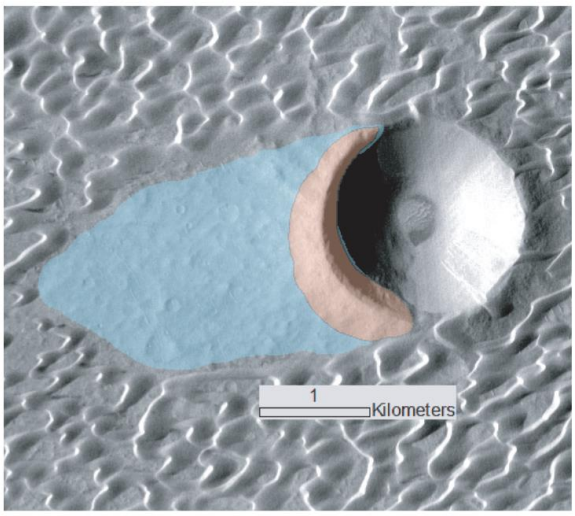

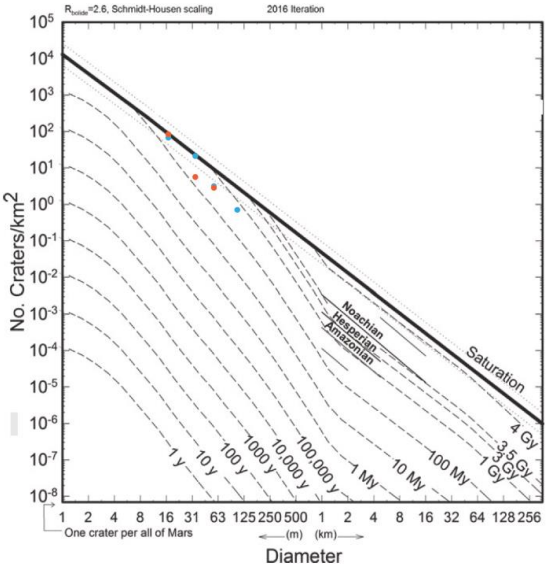

Fig. 5: Left – Indication of large (light blue shading) and small (orange shading) crater-counting areas, and actual crater counts associated with both overlaid on Mars isochrons (from *Hartmann and Daubar*, 2017) Given the small area, the point here is not to determine a precise age for the surface, but to show that a young age on the order of <1 Ma is implausible. CTX base image credit: NASA/JPL/MSSS.

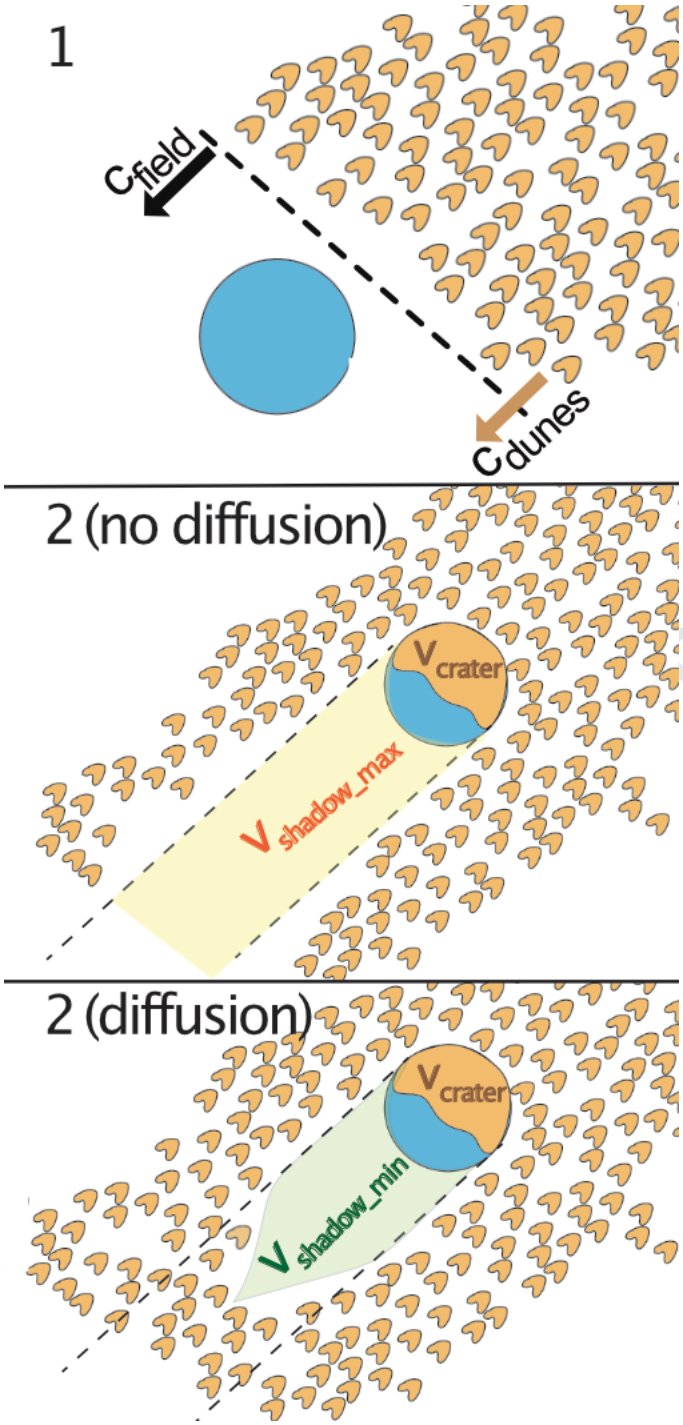

Fig. 6: Cartoon model for the history of crater-dune field interaction at Meroe Patera. The dune field advances in the direction indicated by the black arrows (panel 1) and reaches the crater (2). We illustrate scenarios for the dune field's morphologic evolution in which lateral spreading of sand does/does not occur.

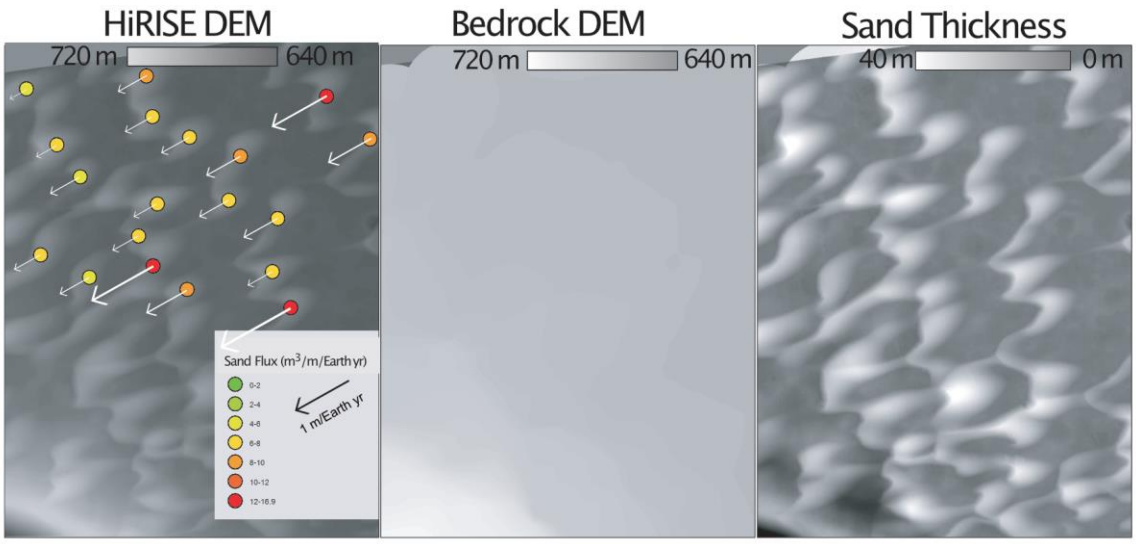

Fig. 7: Left panel – HiRISE DEM generated of the Meroe Patera dune field from HiRISE images ESP_050939_1875 and ESP_051084_1875. Dunes on which sand fluxes were measured are indicated by colored points, with attached vector arrows to indicate magnitudes of sand flux. Middle panel – DEM generated from applying a focal-statistics function to calculate the average bedrock surface height across the dune field. Right panel – DEM indicating sand thickness, generating by subtracting the dataset in the middle panel from the dataset in the left panel. HiRISE image credit: NASA/JPL/University of Arizona.

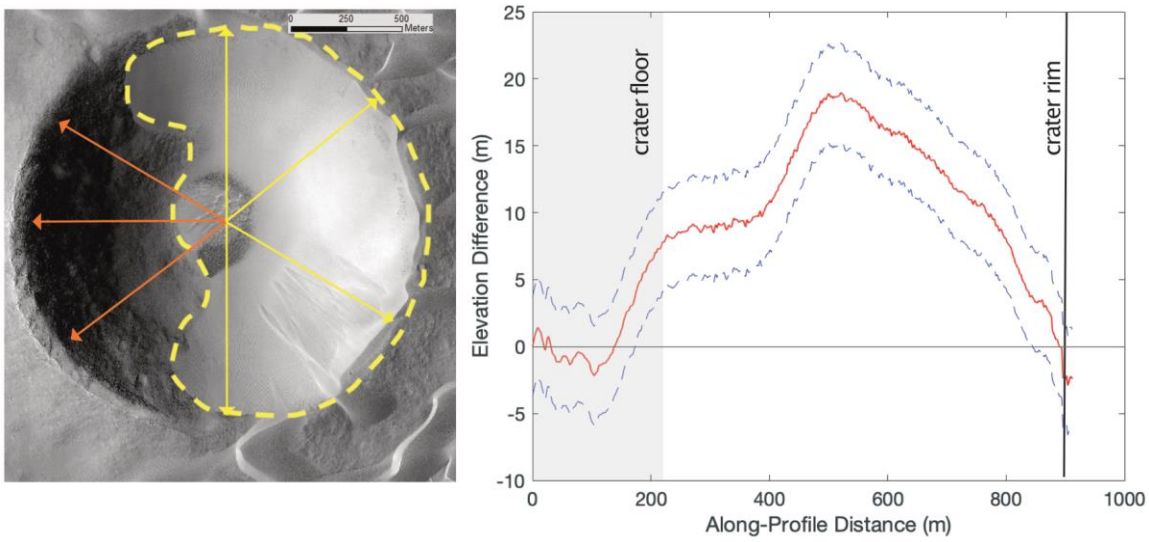

Fig. 8: Left: Imagery of the Meroe Patera crater, with sand-covered areas outlined by a dashed line. Lighter (yellow) arrows indicate sample radial profile lines used in sand-covered areas to derive an average elevation profile for the sand-covered part of the crater; darker (orange) arrows indicate the same for the largely sand-free part. Right: The difference in mean elevation between sand-covered and sand-free parts of the crater, as a function of along-profile distance. 1-sigma uncertainty on the measurement is indicated by the dashed lines. HiRISE base image credit: NASA/JPL/University of Arizona.

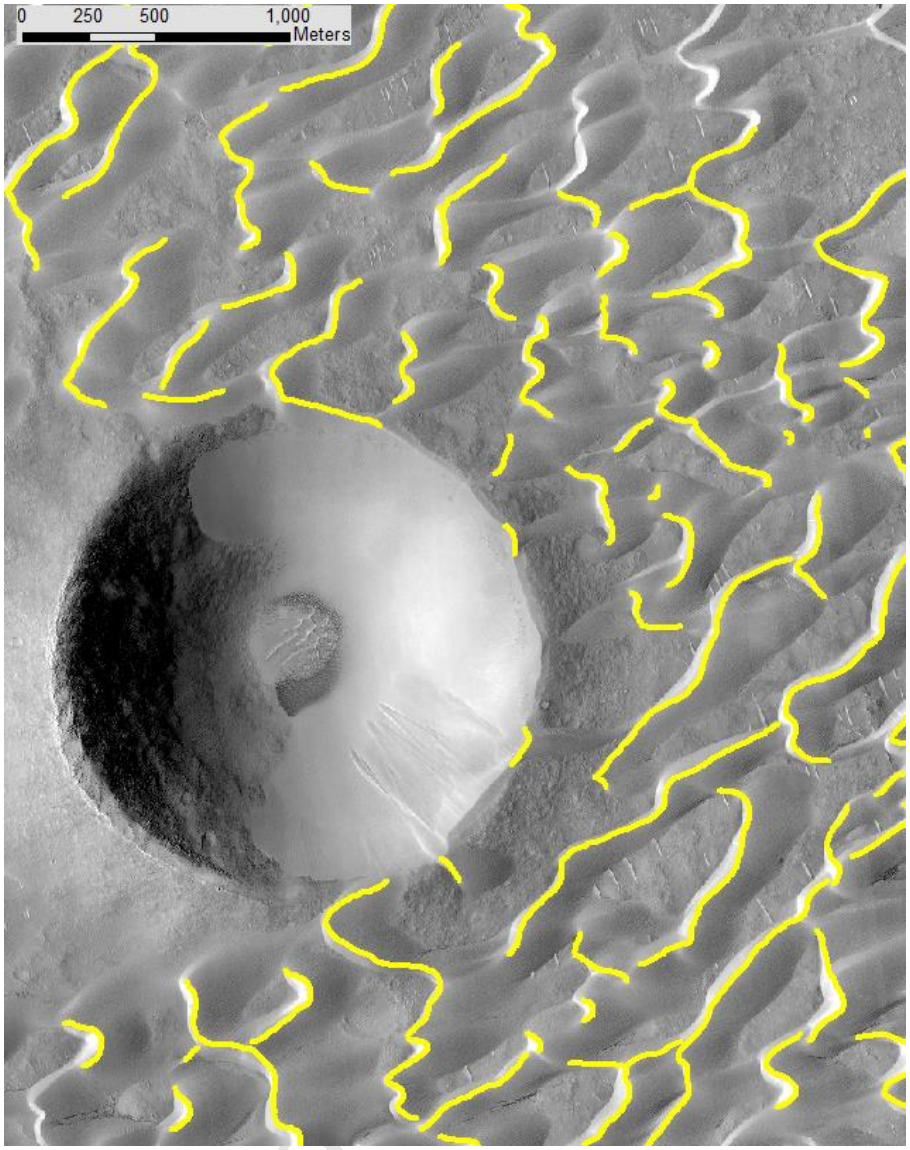

Fig. 9: Mapping of dune brink lines around Nathan's crater. The orientation of dune brink lines does not change systematically near the crater.

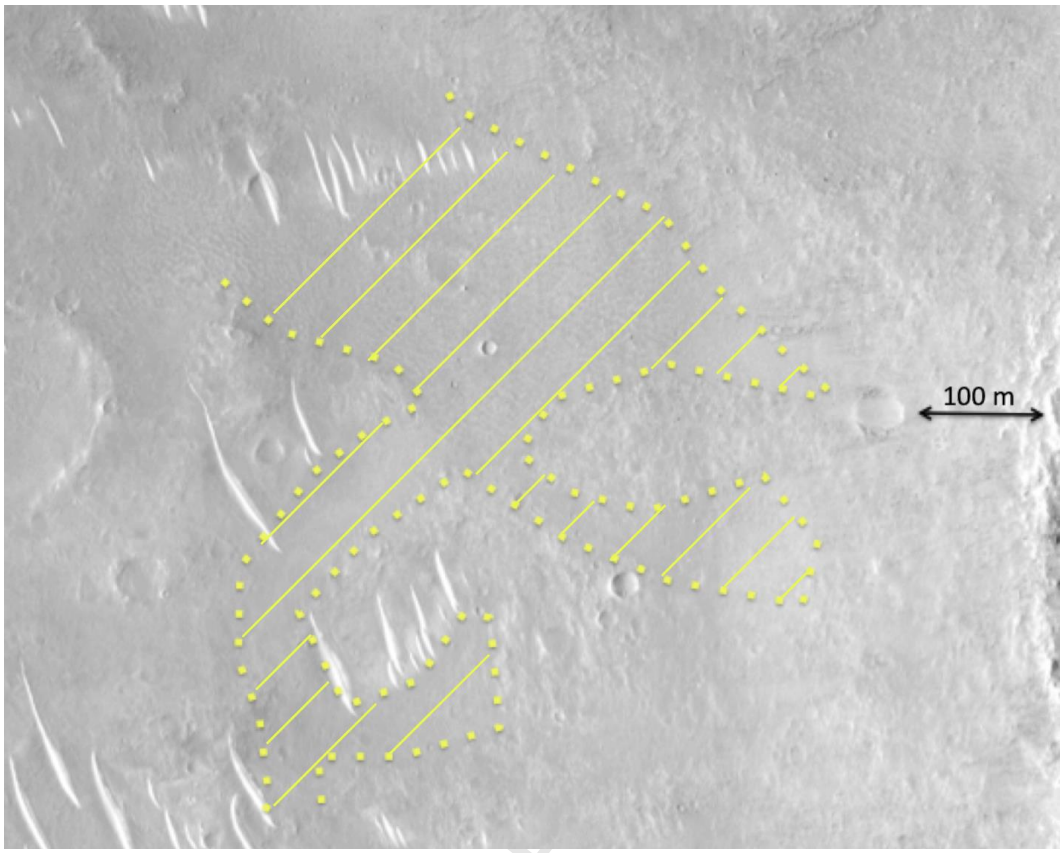

Table 1: HiRISE stereo pairs, from which DEMs were made of sand-free craters used in our evaluation of uncertainty on our assumption of axisymmetric crater geometry. Notes on which craters were used are included. HiRISE image credit: NASA/JPL/University of Arizona.

HiRISE Stereo Pair – Image 1	HiRISE Stereo Pair – Image 2	Notes
ESP_012873_2045	PSP_004052_2045	Largest (>1 km diameter) crater in image
ESP_014011_1315	ESP_014288_1315	Raga Crater (only crater in image)

ESP_025901_2460	ESP_026455_2460	Only crater in image
ESP_027027_2325	ESP_027370_2325	Largest crater in image
ESP_035785_1840	ESP_036062_1840	Largest crater fully contained in image (~800 m diameter)

References

Almeida, M. P., Parteli, E. J. R., Andrade Jr., J. S., and Herrman, H. J., 2008, Giant saltation on Mars: Proceedings of the National Academy of Sciences of the United States of America, v. 105, no. 17, p. 6222-6226, doi:10.1073/pnas.0800202105

Anderson, R. S., 1987, A theoretical model for aeolian impact ripples: Sedimentology, v. 34, no. 5, p. 943-956, doi:10.1111/j.1365-3091.1987.tb00814.x

Andreotti, B., 2004, A two-species model of aeolian sand transport: *Journal of Fluid Mechanics*, v. 510, p. 47-70, doi:10.1017/S0022112004009073

Ayoub, F., Avouac, J.-P., Newman, C. E., Richardson, M. I., Lucas, A., Leprince, S., and Bridges, N. T., 2014, Threshold for sand mobility on Mars calibrated from seasonal variations of sand flux: Nature Communications, v. 5, article 5096, doi:10.1038/ncomms6096

Banks, M. E., Fenton, L. K., Bridges, N. T., Geissler, P. E., Chojnacki, M., Runyon, K. D., Silvestro, S., and Zimbelman, J. R., 2018, Patterns in Mobility and Modification of Middle- and High-Latitude Southern Hemisphere Dunes on Mars: Journal

of Geophysical Research: Planets, v. 123, no. 12, p. 3205-3219, doi:10.1029/2018JE005747

Bridges, N. T., Ayoub, F., Avouac, J.-P., Leprince, S., Lucas, A., and Mattson, S., 2012, Earth-like sand fluxes on Mars: Nature, v. 485, p. 339-342, doi:10.1038/nature11022

Chojnacki, M., Moersch, J. E., and Burr, D. M., 2010, Climbing and falling dune in Valles Marineris, Mars: Geophysical Research Letters, v. 37, doi:10.1029/2009GL042263

Chojnacki, M., Banks, M. E., Fenton, L. K., and Urso, A. C., 2019, Boundary condition controls on the high-sand-flux regions of Mars: Geology, doi:10.1130/G45793.1

Day, M. and Kocurek, G., 2016, Observations of an aeolian landscape: From surface to orbit in Gale Crater: Icarus, v. 280, p. 37-71, doi:10.1016/j.icarus.2015.09.042

Hartmann, W. K., Daubar, I. J., 2017, Martian cratering 11. Utilizing decameter scale crater populations to study Martian history: Meteoritics & Planetary Science, v. 52, no. 3, p. 493-510, doi:10.1111/maps.12807

Hayward, R. K., Fenton, L. K., and Titus, T. N., 2014, Mars Global Digital Dune Database (MGD^3): Global dune distribution and wind pattern observations: Icarus, v. 230, p. 38-46, doi:10.1016/j.icarus.2013.04.011

Kite, E. S., Lewis, K. W., Lamb, M. P., Newman, C. E., and Richardson, M. I., 2013,

Growth and form of the mound in Gale Crater, Mars: Slope-wind enhanced erosion and transport: *Geology,* v. 41, no. 5, p. 543-546, doi:10.1130/G33909.1

Lapotre, M. G. A., Ewing, R. C., Weitz, C. M., Lewis, K. W., Lamb, M. P., Ehlmann, B. L., and Rubin, D. M., 2018: Morphologic Diversity of Martian Ripples: Implications for Large-Ripple Formation, Geophysical Research Letters, v. 45, p. 10229-10239, doi:10.1029/2018GL079029

Leprince, S., S. Barbot, F. Ayoub, and J. P. Avouac (2007), Automatic and precise orthorectification, coregistration, and subpixel correlation of satellite images, application to ground deformation measurements, IEEE Transactions on Geoscience and Remote Sensing, v. 45, no.6, 1529-1558, doi: 10.1073/pnas.0800202105

McEwen, A. S., et al., 2007, Mars Reconnaissance Orbiter's High Resolution Imaging Science Experiment (HiRISE): Journal of Geophysical Research: Planets, v. 112, doi:10.1029/2005JE002605

Melosh, H. J., 1989, Impact cratering: A geologic process, in Research supported by NASA: New York, Oxford University Press, Oxford Monographs on Geology and Geophysics, No. 11, 253 p.

Ould Ahmedou, D., Ould Mahfoudh, A., Dupont, P., Ould El Moctar, A., Valance, A., and Rasmussen, K. R., 2007, Barchan dune mobility in Mauritania related to dune and interdune sand fluxes: Journal of Geophysical Research, v. 112, F02016, doi:10.1029/2006JF000500

Runyon, K. D., Bridges, N. T., Ayoub, F., Newman, C. E., and Quade, J. J., 2017, An

integrated model for dune morphology and sand fluxes on Mars: Earth and Planetary Science Letters, v. 457, p. 204-212, doi:10.1016/j.epsl.2016.09.054

Runyon, K. D., Bridges, N. T., and Newman, C. E., 2017, Martian sand sheet characterization and implications for formation: A case study: Aeolian research, v. 29, p. 1-11

Silvestro, S., Fenton, L. K., Vaz, D. A., Bridges, N. T., and and Ori, G. G., 2010, Ripple migration and dune activity on Mars: Evidence for dynamic wind processes: Geophysical Research Letters, v. 37, doi:10.1029/2010GL044743

Sullivan, R., and Kok, J. F., 2017, Aeolian saltation on Mars at low wind speeds: Journal of Geophysical Research: Planets, v. 122, no. 10, p. 2111-2143, doi:10.1002/2017JE005275

Tanaka, K. L., Robbins, S. J., Fortezzo, C. M., Skinner Jr. J. A., Hare, T. M., 2014, The digital global geologic map of Mars: Chronostratigraphic ages, topographic and crater modification characteristics, and updated resurfacing history: Planetary and Space Science, v. 95, p. 11-24, doi:10.1016/j.pss.2013.03.006

Walker, I. J., 2002, Advances in research on dune-airflow-sand transport dynamics: incorporating secondary flow and sand transport processes: in Proceedings of ICAR5/GCTE-SEN Joint Conference, Lubbock, TX, USA, Publication 02-2, p. 458

Highlights

- A partially sand-filled crater in the active Meroe Patera dune field is accompanied by a dune-free shadow stretching behind it the downwind direction
- We investigate the sand-trapping potential of this crater by comparing its trapped volume of sand to a "missing" volume we would expect to be present in its dune-free shadow behind it if the crater did not exist
- The crater holds much less sand than predicted by missing volume estimates, implying that it is unlikely to be an effective sand trap over long timescales, despite its appearance in modern satellite imagery